Demagnetization Risk Assessment in a Dual Stator Permanent Magnet Vernier Machines

Zia Ullah
Department of Computer, Electrical and Mathematical Science and Engineering
King Abdullah University of Science and Technology (KAUST)
Thuwal, Saudi Arabia
zia.ullah@kaust.edu.sa

Mudassir Raza Siddiqi
Department of Electrical Engineering
Incheon National University
Incheon, South Korea
mudassirrazasid@gmail.com

Shehab Ahmed
Department of Computer, Electrical and Mathematical Science and Engineering
King Abdullah University of Science and Technology (KAUST)
Thuwal, Saudi Arabia
shehab.ahmed@kaust.edu.sa

***Abstract*—As the topologies of permanent magnet vernier machines (PMVM) is getting more complex such as dual rotor and its variants. The thermal, mechanical, and especially demagnetization concern increasing. In this paper, the demagnetization risk evaluation of three similar topologies of dual stator radial type PMVM is presented. Three recently published topologies: dual winding with rotor-yoke, dual winding without rotor-yoke, and single winding without yoke are selected. This design highly improved the torque density and reduced the overall volume. However, the permanent magnets (PMs) in these topologies are at huge risk of irreversible demagnetization. Furthermore, the overall performance of PM-type machines is incomprehensible without a detailed demagnetization analysis. Therefore, a comprehensive mechanical, thermal, and demagnetization analysis considering various operating points and temperatures is conducted to evaluate the risk of demagnetization in these topologies. Finally, some modification are made to optimize of these designs. All analyses are carried out using finite element analysis and co-simulation in ANSYS maxwell and mechanical.**

Keywords—dual stator, permanent magnet vernier machine, demagnetization, analysis.

I. INTRODUCTION

Permanent magnet (PM) type machines have gain popularity due to their compact structure and high torque density [1]. With increasing considerations over various developing applications such as wind power generation and electric vehicles, high-torque performance machines, such transverse flux machines, dual-rotor PM machines [2], harmonic machines [3], and pseudo-PM machines [4] are gaining attractions in the industry as well as in academia. The direct-drive systems, which remove the use of mechanical gears, are considered to be used in high-torque and low-speed applications such as elevators, renewable energy conversion, electric vehicles, and so on. However, the design of regular industrial machines for direct-drive applications may result in very huge structures that can suffer from poor operating characteristics. For example, the transverse flux permanent magnet machine having a high torque density and a pseudo PM machine with quite suitable operating characteristics were introduced in [4]. But these machines have very complex mechanical structures, and a very large volume of magnets was used in these machines, which made them unconventional structures for the direct-drive operations.

Permanent Magnet Vernier machines (PMVM) have been gaining much attraction for direct drive applications due to their high torque density, low cogging torque, and excellent torque performance [5-8]. The operation principle of PMVM is generally based on the flux modulation effect, in which a small rotation of the rotor brings a huge flux change that results in high torque production [9]. They are generally preferred for applications, such as ship propulsion and wind turbine; however, their huge weight and volume prevent their wide acceptance in industrial applications [10].

The PMVM was initially presented in [11], and its design details were discussed in [12]. A major characteristic of the PMVM is high torque density; hence, various high torque density machines are being actively researched. It was proved in [13] that a PMVM can theoretically produce more than twice the back-electromotive force compared to a standard permanent magnet machine due to the flux modulation effect. A comparison between a PMVM and a conventional permanent magnet synchronous machine (PMSM) for wind power application was presented in [14], which shows that the torque performance of the PMVM is better than that of the conventional PMSM having similar volume and outer dimensions. Consequently, various PMVM topologies have been introduced to further increase the torque density. Some major topologies include consequent-pole [15], dual-stator [16-19], and multipole dual-stator designs [20], [21]. Although these designs significantly improve the torque density they have very complex structures and weak mechanical support, particularly, the dual rotor and dual stator. Generally, the PMVM's rotor is comprised of a higher number of rotor poles as compared to the stator of the machine. This results in a higher volume of the magnets and the overall machine manufacturing cost is also increased.

Compared to the single stator PMVMs, the structure of dual stator PMVM is complex, and its mechanical support structure is also difficult. Moreover, since the flux linkage and induced EMF of inner and outer stator windings have some phase shift, the phase windings should be connected in series to avoid the circulating currents, and these connection schemes also introduce additional distributed factors [22]. Furthermore, the dual stator PMVM having a radial type structure always suffers from thermal issues due to inner stator windings. In a dual airgap radial type structure, the inner stator is enclosed inside the rotor. The windings in the inner stator may produce heat during the operations that affect the PMs in the radial structure. To overcome this issue, a topology of dual stator PMVM with single stator excitation was introduced in [10]. In this topology, the winding of the inner rotor was removed and shifted to the outer stator which reduces the thermal stress.

Additionally, a yokeless dual stator structure was introduced in [16] to further improve the torque density. In this topology, the iron core from the rotor was removed which was causing a reduction in the flux linkage between inner and outer stator windings. This strategy improved the volume and torque density remarkably. Similarly, a design combining the

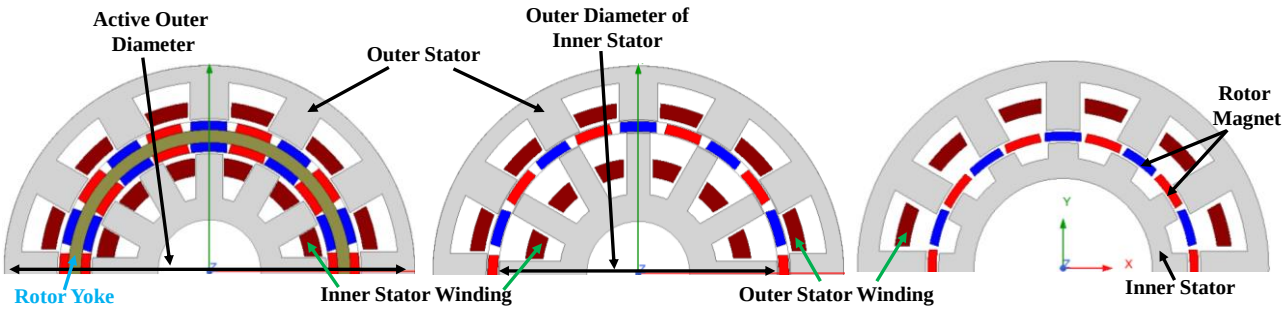

Fig. 1. Topologies of the three PMVMs under study. (a) DSW-Yoke, (b) DSW-Yokeless, (c) SSW.

advantages of yokeless and single stator windings is presented in [23]. This design used a dual stator with a yokeless rotor having single stator windings. The results of this machine were also outstanding in terms of torque density and volume improvement. However, the main disadvantage of Vernier machines is that they use a greater number of magnets than traditional PM-type machines, which not only raises the cost of the machine but also increases the risk of demagnetization. Furthermore, the previously proposed complex topologies made these machines more susceptible to demagnetization, which is rarely highlighted. Machines having complex structure especially with dual windings not only produce more heat but also have less option to manage the heat decipation. PMs are sandwiched in two heat sources in such structures. The high operating temperature severely reduce the residual magnetic flux density of the magnets. The magnets have certain range of reversible demagnetization. If the residual magnetic flux density cross the cuttoff point or the knee point then it entered into irreversible demagnetization region [24]. The irreversible demagnetization (IDF) severely affect the performance of the machine. It increase the losses, cause huge vibration and acustic noise and the machine draws higher current for the demanded load [25]. Therefore, a detailed thermal, mechanical, and demagnetization analysis is necessary to carefully understand the performance of these machines and take step towards thermally and mechanically optimized model to further improve the reliability of PMVMs.

This study conducts a thorough mechanical, thermal, and demagnetization analysis of three recently reported topologies that promised remarkably high flux density relative to their reference model [16], [23]. A dual stator winding with and without a rotor iron-yoke and a single stator yokeless radial flux PMVM topologies are selected for demagnetization analysis. A detailed demagnetization analysis at different operating conditions is conducted and the risk of demagnetization is evaluated in all the models. Suggestion for decreasing demagnetization risk is made for all designs. All the analyses are carried out using the finite element analysis in Ansys Maxwell.

II. DUAL STATOR PMVM TOPOLOGIES

Dual stator vernier machine topologies are appealing due to their high torque density. This paper investigates the demagnetization risk of three identical topologies of dual-stator radial flux PMVMs. The first model, known as dual-stator winding with yoke (DSW-Yoke), has windings on both the inner and outer stators, as well as an iron yoke rotor sandwiched between two stators and two layers of magnets in a back-to-back configuration, Fig. 1(a). It was observed that the presence of iron yoke in the rotor of DSW-yoke not only increases the amount of PMs but also reduces the flow of magnetic flux between the inner and outer stator [23]. Therefore a second variant of the same model, called dual-stator winding yokeless (DSW-Yokeless) is introduced in which the iron yoke has been removed and simply a single layer of magnets were utilized, Fig. 1(b). DSW-Yokeless not only reduced the amount of PMs by 50% but also improved the torque per machine volume by 87%.

Despite the great improvement by DSW-Yokeless, there are significant thermal challenges for the magnets due to the heat produced by the inner rotor windings. Considering this issue, another model is proposed by removing the winding from the inner stator of the previous model and shall be called single stator winding (SSW) from now on, Fig. 1(c). All these steps improved the performance of the machine in terms of torque density. SSW helped in the reduction of heat exerted on magnets as well. All the models have the same outer diameter and the stators, rotors, and magnets are made up of the same material in all the models. The magnets are magnetized radially in all the models. The magnetic volume in the DSW yoke model is higher as compared to the other two models but the thickness of the individual layer of magnets is smaller than in the SSW model. The SSW model has a higher magnet thickness and lesser volume than all the other models. Due to the higher thickness of the magnet layer, the SSW is less prone to demagnetization as explained in the next section. However, all these three models are radial flux and surface type; hence the magnets in all these models seem at great risk of irreversible demagnetization. The application and the operating point of this machine should be carefully observed in order to keep them within safe limits.

The working of the PMVMs is based on the interaction between the magnetic field of PMs and the rotating magnetic field of the stator windings as mentioned in [26]. The relation between the number of stator slots, rotor poles, and stator poles follows the rule mentioned in equation (1):

$$\pm P_s/2 = P_r/2 - S_s \quad (1)$$

Where P_s, P_r, and S_s show stator poles, rotor poles, and stator slots respectively.

The basic design of the presented models was obtained using the mathematical model in [21]. The SSW model was redesigned from the DSW models with further modifications as presented in [20]. The design equations of the PMVM model based on the electromagnetic torque and power as mentioned in [19] are as under:

$$D_{g1}^2 L_{stk} = T_e / [(\sqrt{2}/20)\, \pi^2\, k_w k_\delta\, \alpha_{p1} A B_{g1m}\, (Pr/Ps)\, cos\gamma] \quad (2)$$

$$D_{g1}^2 L_{stk} = P_e / [(\sqrt{2}/10)\, \pi^3\, k_w k_\delta\, \alpha_{p1} A B_{g1m}\, (f/Ps)\, cos\gamma] \quad (3)$$

Where T_e and P_e represent the electromagnetic torque and power of the machine. k, k_w ,k_δ ,α_{p1}, A, B_{g1m}, P_r, P_s, f, D_{g1},L_{stk} and cosγ show the winding factor, leakage factor, rotor pole arc, electrical loading, peak flux density in outer airgap, rotor pole pairs, stator pole pairs, the inner diameter of the outer stator, stack length and the power factor of the machine, respectively.

The working of the PMVMs is generally based on the flux modulation effect. The stator windings generate a low order harmonic field, and the rotor magnetic poles produce the high order harmonic field. These two fields produced by stator windings and the rotor PMs interact to produce the “useful torque”. This effect is termed the "magnetic gearing effect," which results in a high torque production due to a huge flux change by a very small rotation of the rotor.

The detailed parameters of these machines are given in Table I. The inner and outer stator has 12 slots and a three-phase distributed type winding having a 4 poles configuration. The rotor contains 20 poles of NdFeb magnets and non-magnetic support is used in the yokeless rotor models to the magnets in place.

TABLE I. PARAMETERS OF ALL THREE DESIGNS

Parameter	Unit	Values		
		DSW-Yoke	*DSW-Yokeless*	*SSW Model*
Active Outer Diameter (D_o)	mm	120		
Active Inner Diameter (D_i)	mm	30		52
Outer Diameter of the inner stator	mm	68.8	81.1	72.7
Active Axial Length	mm	100		
Number of Rotor Pole Pairs	-	10		
Number of Stator Slots	-	12		
Number of Stator poles	-	4		
Length of Air Gap	mm	0.7		
Magnet Type	-	NdFeb (Br=1.23 T, Hc=-890 kA/m)		
Rotor Core Material	-	SUS304		
Volume of Magnet	L	0.105	0.072	
Machine Volume	L	1.06		0.92
Number of conductors per Slot (outer/inner)	-	70/70		140
Slot Fill Factor (Outer/Inner Stator)	%	50/60	50/50	50
Rated Rotational Speed	rpm	400		
Phase Current	A_{rms}	4.7		

III. MECHANICAL ANALYSIS OF PMVM MODELS

The cross-sectional 3D views of the dual stator single rotor PMVM model having DSW yokeless topology and the SSW topology are shown in Fig. 2 and Fig. 3, respectively. The red color in the figures shows the magnets in the yokeless rotor support cage and the gray color shows the support structures for the rotor and stators.

The DSW yoke and yokeless topologies have the same dimensions and mechanical configuration where one end of the rotor is open and the other end is closed as shown in Fig. 2. The only difference between the two topologies is the absence of a rotor core and one layer of magnets in the yokeless model. According to Fig. 2, the rotor in the DSW model has a U-shape structure, where one end (down) is connected to the shaft for load connections, and the other end (up) is open to allow the winding terminals to connect between the two stators. This type of rotor structure could have a risk of vibrations during the routine operation of the machine in the load conditions and it could have a possible risk of demagnetization due to the vibrations.

On the other side, the SSW model shown in Fig. 3 contains a closed shape rotor that is connected to the central shaft via a support bearing. The inner stator is not having any windings, so the rotor can be closed at both ends and connected to the shaft similar to the conventional radial type rotor structures. This closed drum-shaped structure allows the rotor to rotate without the risk of possible vibrations during load operations and hence the risk of demagnetization is also much reduced in the case of the SSW model as compared to the DSW models having yoke and yokeless structures.

The mechanical stress analysis on the moving parts of the models was performed using the co-simulations between Ansys Maxwell and Ansys Mechanical. The mechanical stress analysis results on the rotor support structure of all the models are shown in Fig. 4. The maximum principal stress on the rotor core of the DSW yoke and yokeless model is same due to the same configuration of the rotor core in both models. It can be seen that the mechanical stress on the DSW models is higher as compared to the SSW model. The higher stress on the rotor

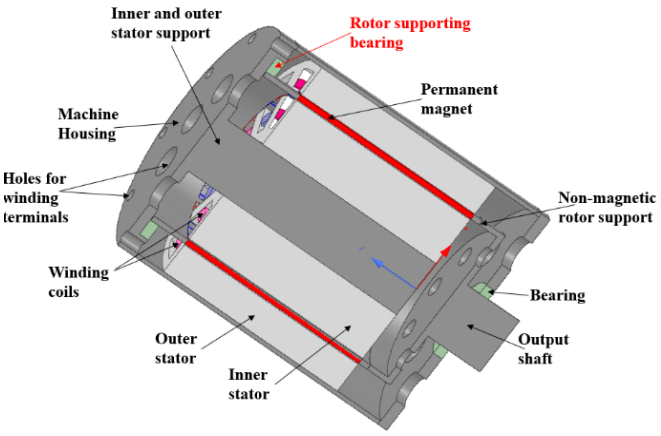

Fig 2. Cross-sectional view of PMVM DSW-yokeless model

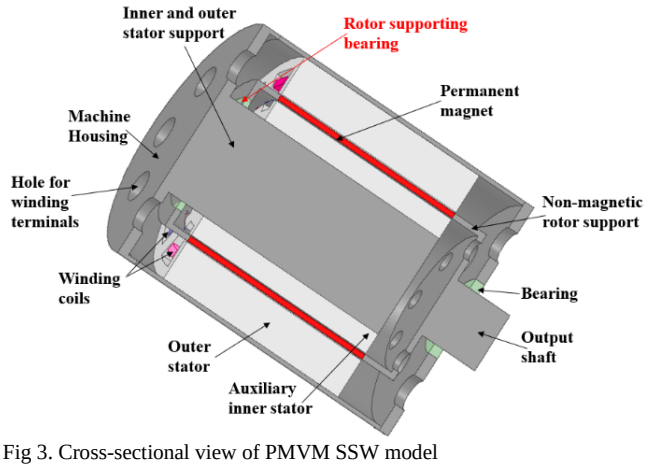

Fig 3. Cross-sectional view of PMVM SSW model

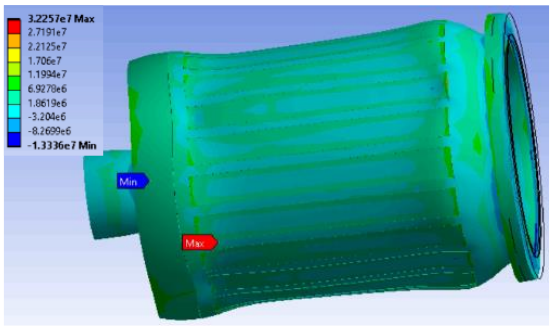

(a)

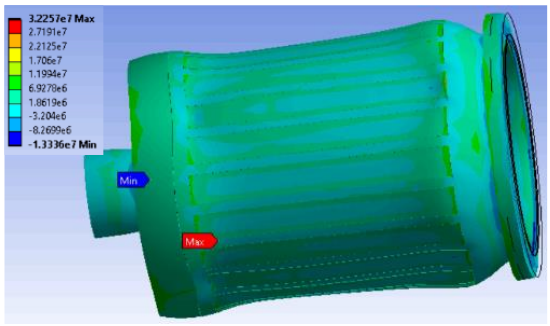

(b)

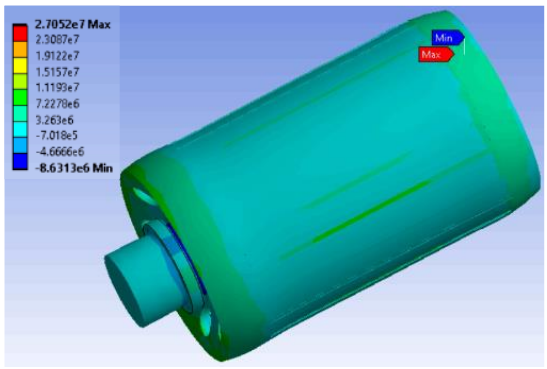

(c)

Fig. 4. Mechanical analysis of rotating part of Dual airgap PMVM (a) DSW yoke (b) DSW yokeless. (c) SSW yokeless.

core can in turn increase the pressure on the magnet layers attached to the rotor cores and finally may increase the risk of damage and demagnetization in the magnets as well. On the other hand, as shown in Fig. 4(c), the SSW model's rotor core shows relatively less principle mechanical stress and hence made it a better structure compared to DSW models.

IV. Therml Analysis of PMVM

The thermal performance of a machine is the most essential component in machine design. It must be ensured that the heat created inside the machine does not harm the insulation of the windings or, more crucially, the permanent magnet in the rotor. Furthermore, the thermal analysis is a prerequisite for the demagnetization analysis. It is quite difficult to establish an accurate temperature of the permanent magnet in real time. The thermal analysis in this study is carried out using a co-simulation of the FEM model and Ansys mechanical at full load and ambient temperature (20°C). The thermal analysis results of the PMs of the outer layer of the DSW-Yoke model, DSW yokeless model, and SSW yokeless model are shown in Fig. 5. The maximum temperature of PMs in the DSW yoke and DSW yokeless models was approximately 40°C, but the maximum temperature in the SSW yokeless model was around 37°C. This is because the inner stator has no winding. The SSW model also has a lower minimum temperature than the other two models. It may be inferred that SSW is more stable in terms of the machine's thermal features.

Thermal analysis results are affected by the reference temperature, type of cooling system, and convection coefficient. In addition, the worst-case scenario should be investigated. To replicate the worst-case situation, we must choose the ambient temperature based on the environment in which the machine is running. Temperatures in the environment can frequently reach 40 to 45 degrees Celsius. If you take this temperature range to be the ambient temperature. In a natural cooling system, the temperature of the magnets in the benchmark PMVM can easily approach 80°C. Temperatures can even exceed this limit in some situations.

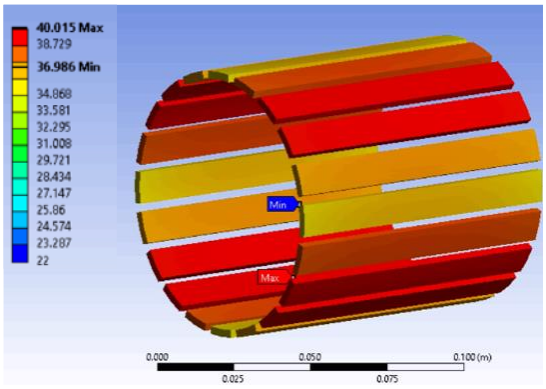

(a)

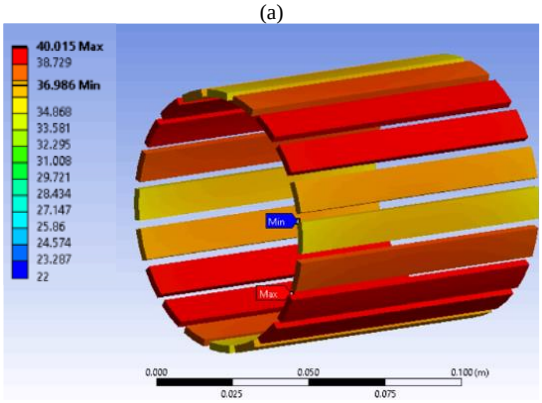

(b)

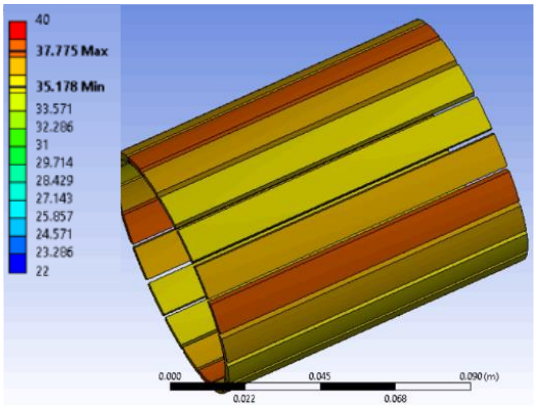

(c)

Fig. 5. Thermal Analysis of PMs for for (a) outer layer of DSW-yoke (b) DSW-yokeless (c) SSW-Yokeless PMVM.

V. DEMAGNETIZATION ANALYSIS

Demagnetization happens when the strength or residual magnetic flux density of a PM is permanently reduced by an external magnetic field and does not recover even after the external field is removed. High temperature, aging, physical damage, and severe flux weakening are all factors that contribute to PM demagnetization [27]. Demagnetization has a significant impact on machine performance. It not only increases losses, vibration, and acoustic noise, but it can also cause other types of faults as winding short fault [28]. The operating temperature and load of the machine are crucial in PM demagnetization. The machine's performance degrades as the temperature rises. Temperature has a direct impact on both winding and PM performance. In this study, N35 grade permanent magnet is used. Fig. 6 depicts the N35 grade magnet's characteristic curve. At 60°C, the cutoff or knee point is somewhat higher than 1k Gauss or 0.1T. At 80°C, the knee point is slightly higher than 2k Gauss, or 0.2T. PMVMs are typically the best options for wind turbines. The maximum operating temperature of a wind turbine generator is typically between 50 and 70°C [23]. Keeping this temperature range in mind, simulations were performed at 60°C and with a worst-case scenario of 80°C in this analysis.

The FEM findings of magnetic flux density distribution at PMs for all three models are presented in Fig. 7(a), (b), and (c) for the DSW-yoke, DSW-yokeless, and SSW models, respectively. For a fair comparison of all models, the findings are given on the same scale. The weakest locations (those with the lowest flux density) are highlighted, and the variation of the magnetic flux density at these sites with the demagnetization curve is illustrated in Fig. 7. The BH curve is derived from the magnet's datasheet, and the demagnetization curve is obtained after demagnetization study of the three models using FEM analysis.

The highest temperature in this investigation is set at 80°C as explained in earlier section. To accurately examine demagnetization, the weakest spots on the magnets are found using FEA, and then different points on the PMs of machines are selected for investigation, Since all the three topologies of the benchmark machines have radial flux, only the radial component of the magnetic flux intensity (H_{radial}) and density (B_{radial}) given in (1) and (2) will contribute to demagnetization. Where H_{xy} and B_{xy} are the x- and y-axis components of the PM flux intensity and density, respectively. θ is the angle between magnetization angle and x-axis of phase-A.

$$H_{radial} = H_x cos\theta + H_y sin\theta \quad (1)$$

$$B_{radial} = B_x cos\theta + B_y sin\theta \quad (2)$$

The radial component of the magnetic field and magnetic flux density is calculated using FEM simulation simulation using equation (1) and (2).

The magnetic flux density variation at the weakest spots are observed at 60 and 80 degrees celsius while the machine was operating at rated speed and load. At 60°C, the magnetic flux density of DSW-Yoke model is above the knee point (K_1) as shown in Fig. 8, however the DSW-yokeless and SSW models are below the K_1 indicating that they are irreversibly demagnetized even at 60°C, as shown in Fig. 9. The severity of the demagnetization is minor, but if it continues for an extended period of time, the severity may rapidly increase

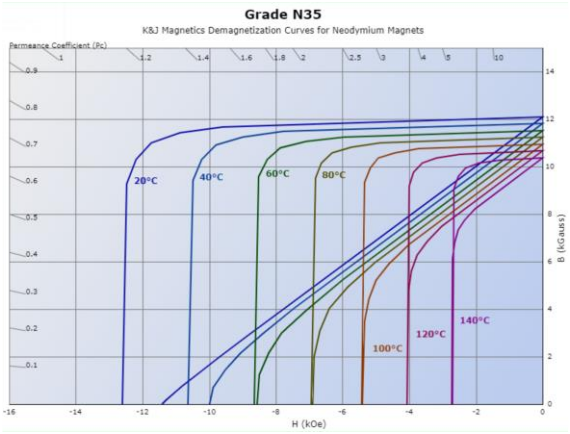

Fig. 6. Characteristic curve of the N35 grade permanent magnet.

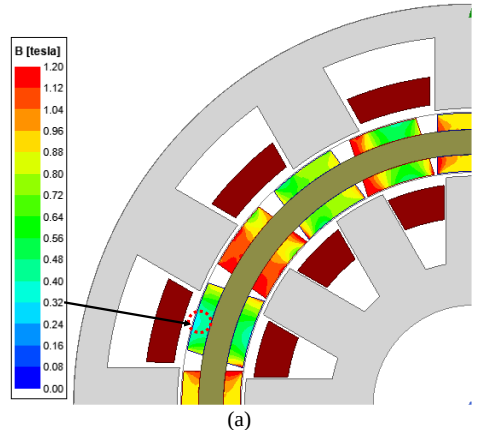

(a)

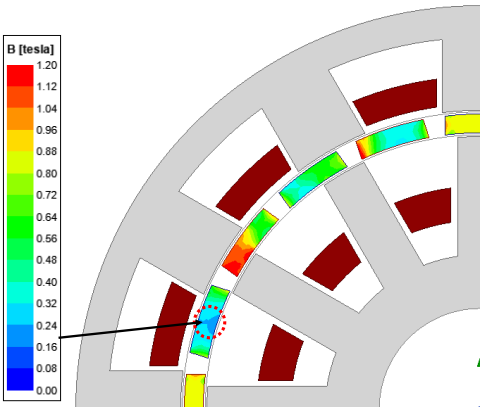

(b)

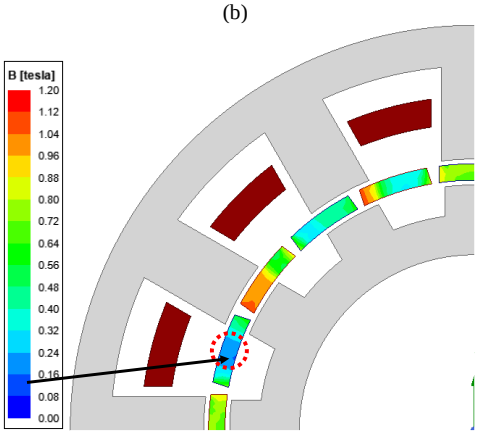

(c)

Fig.7. Magnetic flux density distribution in permanent magnets. (a) DSW-yoke model, (b) DSW-Yokeless model, (c) SSW model.

even with the same operating temperature. Furthermore, the same analysis was repeated at 80ºC just to check the reliability of these models. The results demonstrate that at 80ºC, the

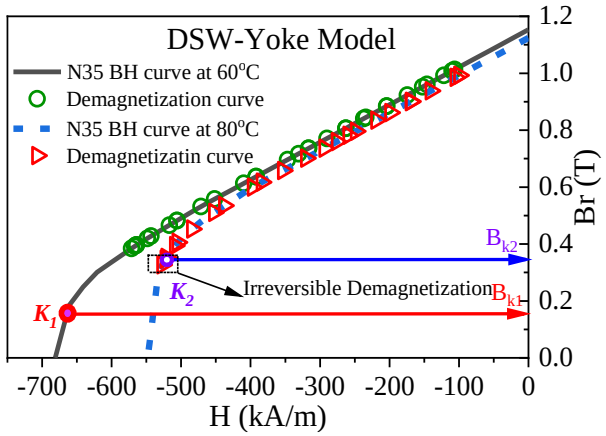

Fig. 8. Demagnetization curve of DSW-Yoke base model.

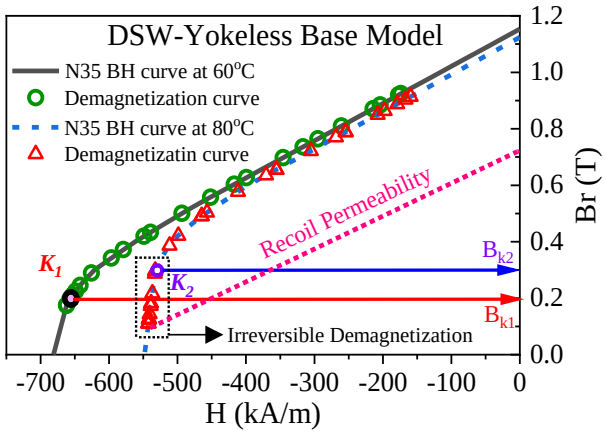

Fig. 9. Demagnetization curve of DSW-Yokeless base model.

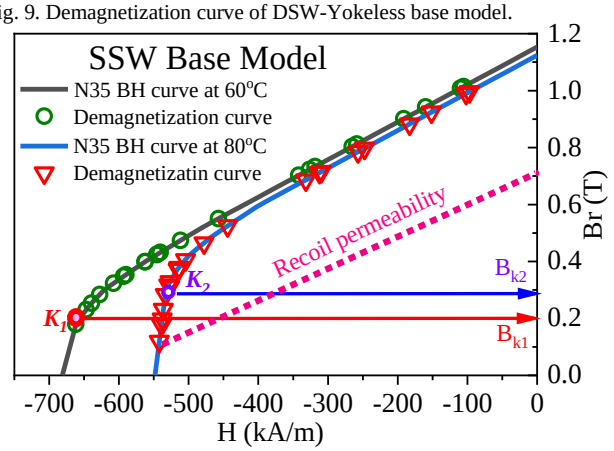

Fig. 10. Demagnetization curve of SSW base model.

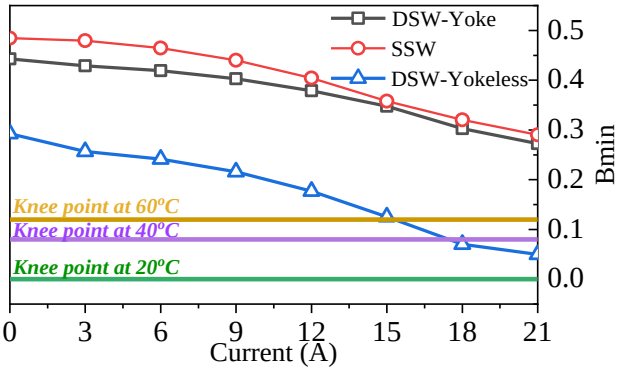

Fig. 11. B_{min} variation at different stator current.

the DSW-Yoke model's minimum magnetic flux density is just near the knee point, indicating that demagnetization will occur soon under the same operating conditions, as shown in Fig. 8. The DSW-yokeless and SSW models, on the other hand, were extensively demagnetized (Figs. 9 and 10). It can be shown that the recoil premebility in this state approaches 0.7T, indicating over 40% demagnetization. Similar performance was shown by the SSW model as well. The DSW-yoke model outperforms the DSW-yokeless and SSW models. Even at 60ºC, the DSW-yokeless and SSW models would not survive. Any additional stress during the transient will result in substantial demagnetization.

The models under consideration were said to be optimum in terms of torque density and volume. However, all of these models required optimization to account for the demagnetization impact. The outer layer of the PMs is more prone to demagnetization in the DSW-Yoke model due to stronger flux linkage. Increasing the thickness of PMs reduces the risk of demagnetization and allows it to operate at higher temperatures of up to 90ºC. DSW-yokeless and SSW designs were modified. To maintain a fair comparison and regulate the motor's cost, the thickness of the magnet in both topologies was increased while the breadth of the magnet was reduced. As a result, the demagnetization performance of the SSW design, as shown in Figs. 12 and 13, was significantly enhanced. At 60ºC, there was also a significant improvement in the DSW-yokless model (Fig. 13). (a). However, at 80ºC, the improvement was ineffective. The minimal flux density is still close to the knee point. It demonstrates that the yokeless model with double winding does not appear to be a particularly good design in terms of demagnetization. SSW, on the other hand, performed well at both 60ºC and 80ºC (Fig. 13). (b). The operation point is visible above the knee. Figure 14 depicts a comparison of the PM losses for the benchmark three topologies and the improved models. It is clear that after optimization, the PM losses in the yoke and SSW models have improved. Fig. 15 also depicts the core loss comparison. A similar upward trend in core loss can be observed. Finally, Fig. 16 depicts the electromagnetic torque comparison. The torque of the DSW-yoke model was somewhat lowered during optimization, but the torque ripple rose dramatically. The torque of the SSW model, on the other hand, remains nearly the same, making the SSW model the most appealing of these three topologies. In terms of PM volume, motor volume, and torque density, the SSW model already has a significant advantage over the other two variants.It has satisfying result in term of demagnetization as well. Moreover, any electrical machine should be able to withstand at least three times its rated current. The variation in minimum flux density (B_{min}) of PMs at different currents was compared in Fig. 11. It can be seen that the B_{min} of the DSW-Yoke and SSW models is higher than the knee point at 60ºC, however, the B_{min} of the DSW-Yokeless model is lower than the knee point even at 40ºC.

It is quite difficult to make further adjustments to the thickness of PM given the constraints of slot size and windings in order to optimize the DSW-yokeless model. To address this issue, one possibility is to change the grade of magnet, such as utilizing a N35UH type magnet, which may be suitable for this design. N35UH and other related magnets can resist higher temperatures. If N35UH or another equivalent grade of magnet is used in certain machine topologies, the machine will be safe even if it is working at 100 ºC. However, it may have other limitations, such as significantly increasing the machine's cost. Because the amount of PM in PMVMs is

much higher than in conventional PMSMs. Finally, following careful examination, it was determined that the extremely significant torque density improvements in the benchmark topologies came at the expense of demagnetization danger. It is concluded that the demagnetization risk should be seriously considered in dual stator machines in general. To avoid potential demagnetization, a specific cooling system must be installed to keep the temperature within a particular range at all times.

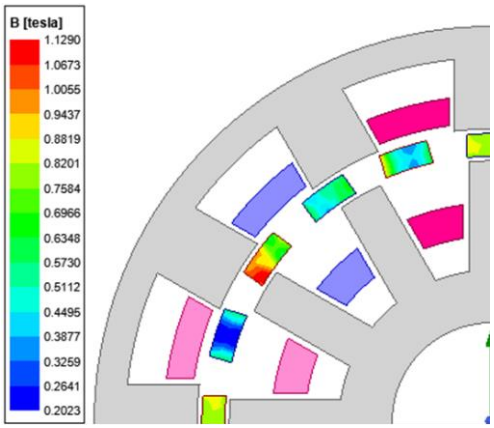

(a)

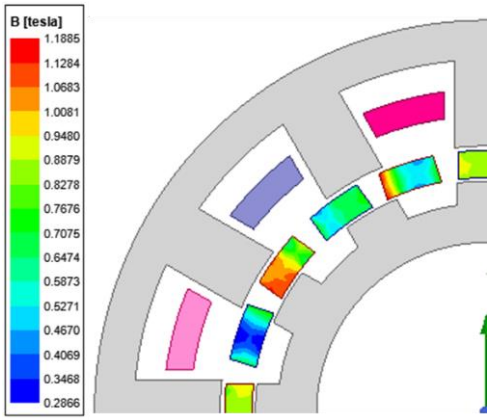

(b)

Fig.12. Magnetic flux density distribution of optimized models at 60ºC. (a) DSW-Yoke model, (b) SSW model.

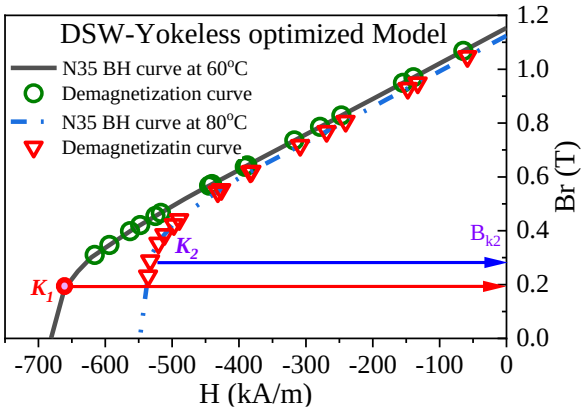

(a)

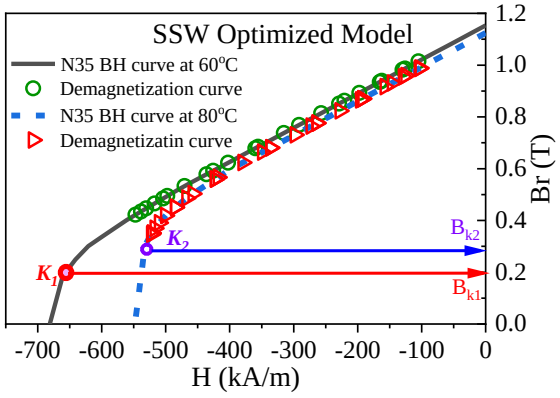

(b)

Fig. 13. Demagnetization curve of the optimized models. (a)DSW-Yoke, (b) SSWmodel.

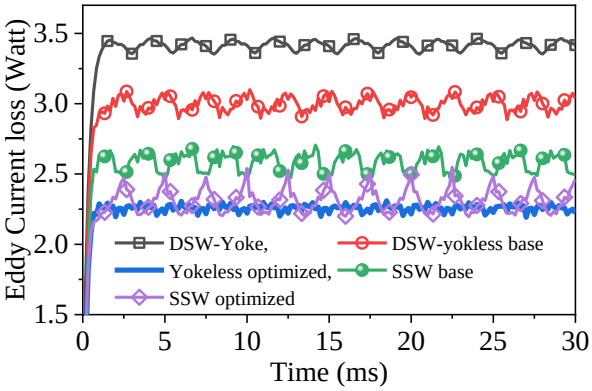

Fig. 14. Eddy current loss of all three topologies along with the optimized models.

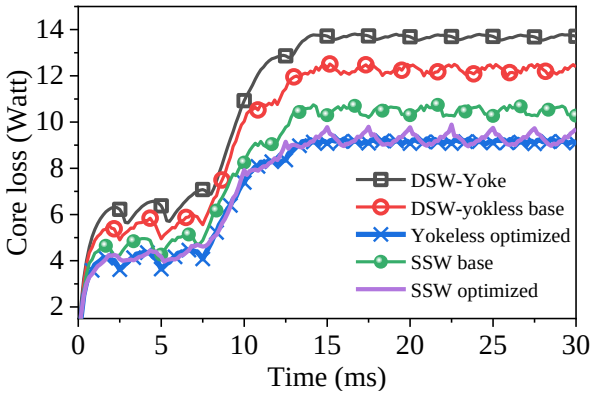

Fig. 15. Core loss comparison of all three topologies along with optimized models.

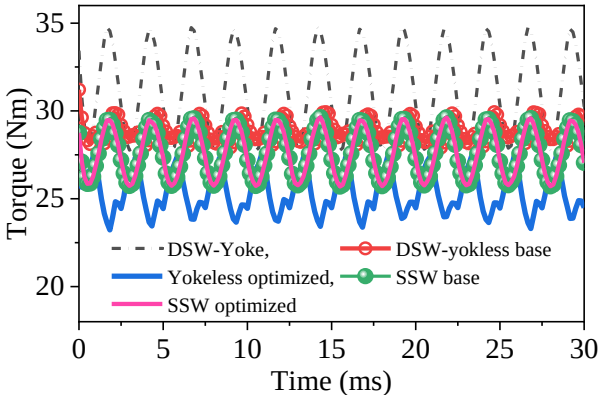

Fig. 16. Electromagnetic torque comparison of based and all the three along with optimized models.

VI. Conclusions

A detailed mechanical, thermal and demagnetization of a dual airgap radial type permanent magnet vernier machine is presented. Three topologies are investigated and compared for the demagnetization: dual-stator PMVM with a rotor yoke, dual-stator dual winding PMVM with a yokeless rotor, and dual-stator single winding PMVM with a yokeless rotor. Mechanical stress for all topologies are compared followed by the temperature of the PMs during operation were calculated. The impact of load and temperature on the permanent magnets (PMs) of the machines are studied and the potential health condition under different operating condition was studied in detail. It was found that all the DSW-yokless and SSW models are demagnetized in its current form. Some modifications were made to optimized these design. The DSW-yoke model is acceptable but need to be carefully operate. The SSW design after optimization became the best design interms of performance, structure and cost.

References

[1] Z. Ullah and J. Hur, "Analysis of inter-turn-short fault in an FSCW IPM type brushless motor considering effect of control drive," *IEEE Transactions on Industry Applications*, vol. 56, no. 2, pp. 1356-1367, 2019.

[2] R. Qu and T. Lipo, "Dual-rotor, radial-flux, toroidally wound, permanent magnet machines," *IEEE Trans. Ind. Appl*., vol. 39, no. 6, pp. 1665–1673, Nov./Dec. 2003.

[3] L. Jian, G. Xu, C. Mi, K. Chau, and C. Chan, "Analytical method for magnetic field calculation in a low-speed permanent magnet harmonic machine," *IEEE Trans. Energy Convers*., vol. 26, no. 3, pp. 862–870, Sep. 2011.

[4] K. Atallah, J. Rens, S. Mezani, and D. Howe, "A novel 'pseudo' direct drive brushless permanent magnet machine," *IEEE Trans. Magn*., vol. 44, no. 11, pp. 4349–4352, Nov. 2008.

[5] A. Toba and T. Lipo, "Generic torque-maximizing design methodology of surface permanent-magnet vernier machine," *IEEE Trans. Ind. Appl*., vol. 36, no. 6, pp. 1539–1546, Nov./Dec. 2000.

[6] L. Wei and T. Nakamura, "A Novel Dual-Stator Hybrid Excited Permanent Magnet Vernier Machine With Halbach-Array PMs," in *IEEE Trans. on Magn*., vol. 57, no. 2, pp. 1-5, Feb. 2021

[7] Siddiqi, M.R., Ullah, Z. & Hur, J. "Torque characteristics analysis of dual-airgap spoke-type permanent-magnet Vernier machine considering pole ratio effect" Springer Electr. Eng., vol 102, pp. 1405–1412, Feb. 2020.

[8] Li, D., Qu, R., Lipo, TA: 'High-power-factor Vernier permanent-magnet machines', *IEEE Trans. Ind. Appl*., 2014, 50, (6), pp. 3664–3674.

[9] T. Zou, D. Li, R. Qu, D. Jiang, and J. Li, "Advanced high torque density PM Vernier machine with multiple working harmonics," *IEEE Trans. Ind. Appl*., vol. 53, no. 6, pp. 5295–5304, Nov./Dec. 2017.

[10] A. Ishizaki, T. Tanaka, K. Takasaki, and S. Nishikata, "Theory and optimum design of PM Vernier motor," *in Proc. 7th Int. Conf. Elect. Mach. Drives, Durham, U.K*., Sep. 1995, pp. 208–212.

[11] S.Ho, S. Niu, and W. Fu, "Design and comparison of vernier permanent magnet machines*," IEEE Trans. Magn*., vol. 47, no. 10, pp.3280-3283, Oct.2011.

[12] N. Baloch, B. Kwon and Y. Gao, "Low-Cost High-Torque-Density Dual-Stator Consequent-Pole Permanent Magnet Vernier Machine," *in IEEE Transactions on Magnetics*, vol. 54, no. 11, pp. 1-5, Nov. 2018.

[13] Du, Z.S., Lipo, TA: 'Torque performance comparison between a ferrite magnet Vernier motor and an industrial interior permanent magnet machine', *IEEE Trans. Ind. Appl*., 2017, 53, (3), pp. 2088–2097.

[14] K. Xie, D. Li, R. Qu, and Y. Gao, "A novel permanent magnet Vernier machine with Halbach array magnets in stator slot opening," *IEEE Trans. Magn.*, vol. 53, no. 6, Jun. 2017, Art. no. 7207005.

[15] Tlali, P.M.; Wang, R.-J.; Gerber, S. Comparison of PM Vernier and Conventional Synchronous 15 kW Wind Generators. *In Proceedings of the 2018 XIII International Conference on Electrical Machines (ICEM)*, Alexandroupoli, Greece, 3–6 September 2018; pp. 2065–2071.

[16] Siddiqi, Mudassir R., Tanveer Yazdan, Jun-Hyuk Im, Muhammad Humza, and Jin Hur. 2021. "Design and Analysis of a Dual Airgap Radial Flux Permanent Magnet Vernier Machine with Yokeless Rotor" *Energies* 14, no. 8: 2311.

[17] Siddiqi M.R., Khaliq S., Kwon J.W., Kwon B.I., 'Optimal Design of Dual Stator Spoke Type Vernier Machine Considering Armature Winding Placement'. *In International Journal of Applied Electromagnetics and Mechanics*, vol. 59, no. 3, pp. 921-930, 2019

[18] N. Baloch, S. Khaliq, and B. I. Kwon, "HTS dual-stator spoke-type linear Vernier machine for leakage flux reduction," *IEEE Trans. Magn*., vol. 53, no. 11, Nov. 2017, Art. no. 8111104.

[19] F. Chai, S. Cui, and S. Cheng, "Performance analysis of double-stator starter generator for the hybrid electric vehicle," *IEEE Trans. Magn*., Jan. 2005 vol. 41, no. 1, pp. 484–487.

[20] Wei, L.; Nakamura, T. A Novel Dual-Stator Hybrid Excited Permanent Magnet Vernier Machine with Halbach-Array PMs. *IEEE Trans. Magn.* 2021, 57, 1–5.

[21] S. Niu, S. L. Ho, and W. N. Fu, "A novel direct-drive dual-structure permanent magnet machine," *IEEE Trans. Magn*., vol. 46, no. 6, pp. 2036–2039, Jun. 2010.

[22] D. Li, R. Qu, W. Xu, and J. Li, "Design procedure of dual-stator, spoke array vernier permanent magnet machines," *IEEE Trans. Ind.Appl*., vol. 51, no. 4, pp. 2972-2983, July-Aug. 2015.

[23] M. R. Siddiqi, T. Yazdan, J. -H. Im, Y. -K. Lee and J. Hur, "Dual Stator Permanent Magnet Vernier Machine With Yokeless Rotor Having Single Stator Winding for Torque Density Improvement," in *IEEE Access*, vol. 9, pp. 151155-151166, 2021.

[24] Z. Ullah and J. Hur, "Irreversible Demagnetization Fault Prognosis in a Permanent Magnet type Machines," *2020 IEEE Energy Conversion Congress and Exposition (ECCE)*, 2020, pp. 742-747.

[25] Z. Ullah, S. Lee, M. R. Siddiqi and J. Hur, "Online Diagnosis and Severity Estimation of Partial and Uniform Irreversible Demagnetization Fault in Interior Permanent Magnet Synchronous Motor," *2019 IEEE Energy Conversion Congress and Exposition (ECCE)*, 2019, pp. 1682-1686.

[26] Y. Gao, R. Qu, D. Li, H. Fang, J. Li, and W. Kong, "A novel dual-stator Vernier permanent magnet machine," *IEEE Trans. Magn.*, vol. 53, no. 11, Nov. 2017, Art. no. 8110105.

[27] Ullah, Zia, and Jin Hur. 2018. "A Comprehensive Review of Winding Short Circuit Fault and Irreversible Demagnetization Fault Detection in PM Type Machines" *Energies* 11, no. 12: 3309.

[28] Z. Ullah, S. Lee and J. Hur, "A Torque Angle-Based Fault Detection and Identification Technique for IPMSM," in *IEEE Transactions on Industry Applications*, vol. 56, no. 1, pp. 170-182, Jan.-Feb. 2020.